Perspectives on the Development of Elastography

2

Kevin J. Glaser and Richard L. Ehman

Introduction

Diagnostic medicine involves a synthesis of information about the current and past health of a patient which is used to diagnose the patient's condition and to design a plan for future medical care and treatment. This information can come from many sources, including discussions about family medical history to indicate hereditary conditions, the results of blood and culture tests to indicate the presence of known pathogens and to assess the chemical and cellular balance of the patient, and the results of imaging tests (e.g., X-ray and MRI) to determine abnormalities in the structure and function of particular organs. A common technique used in routine physical examinations is palpation [1, 2]. Among its numerous uses, palpation allows physicians to assess changes in the mechanical properties of tissue associated with the presence and development of certain diseases. Breast and thyroid cancer, for example, are often detected as a stiffening of normally soft glandular tissue [3]. Similarly, liver disease often results in cirrhosis of the liver, a condition recognized by a marked increase in the stiffness of the entire liver [4].

The power and utility of palpation can be seen in reports that many breast cancers are detected by palpation before being found using mammography, and some cancers detected using palpation are even occult on mammography [5–7]. Similarly, abdominal tumors are often found during surgery that were not detected earlier by CT, MRI, or ultrasound [8]. While palpation continues to be an important tool for clinicians, it is still a qualitative technique that is limited to tissue accessible by the physician. The use of imaging techniques designed to quantitatively assess the mechanical properties of tissue, even tissue not directly accessible by touch, could provide significant information to physicians. Since there are known changes in the mechanical properties of tissue associated with the advanced stages of many diseases, it is likely that there are changes to tissue that occur at even earlier stages of these diseases that may be useful for diagnosing the disease, predicting the course of the disease, and monitoring the effect of treatment.

Modern medical imaging has become an invaluable tool for assessing the structure and function of healthy and diseased tissue in vivo and noninvasively. For example, techniques such as film radiography, CT, MRI, PET, SPECT, and ultrasonography can provide information about bone fractures, tissue degeneration, abnormal blood flow and perfusion, and tumor location and margins. Each of these techniques relies on

K.J. Glaser, Ph.D. (✉) • R.L. Ehman, M.D.
Department of Radiology, Mayo Clinic College of Medicine, Mayo Clinic, Rochester, MN, USA
e-mail: Glaser.Kevin@mayo.edu; Ehman.Richard@mayo.edu

S.K. Venkatesh and R.L. Ehman (eds.), *Magnetic Resonance Elastography*,
DOI 10.1007/978-1-4939-1575-0_2,

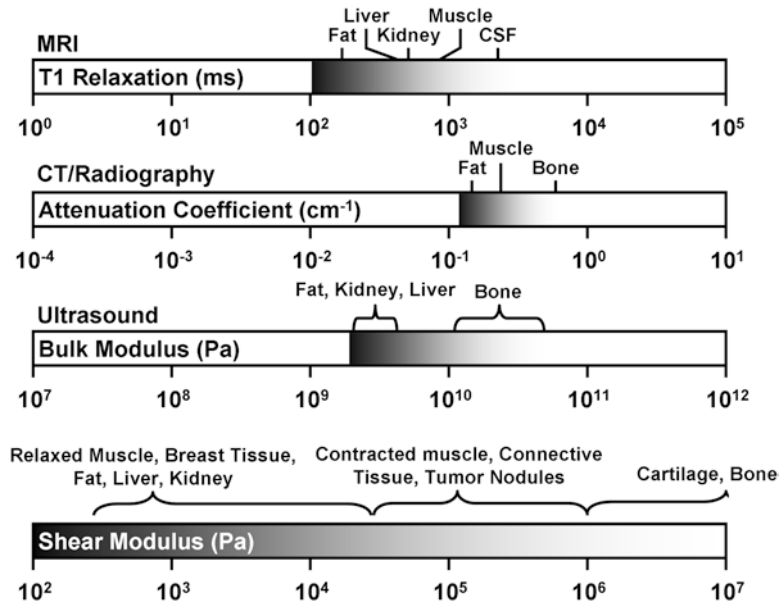

Fig. 2.1 Examples of tissue properties responsible for contrast in imaging techniques including MRI, CT, and ultrasonography. The T1 relaxation rate, X-ray attenuation coefficient, and bulk modulus of soft tissues vary over about one order of magnitude. The shear modulus, a measure of tissue stiffness, varies by several orders of magnitude for healthy and pathologic tissues

differences in specific properties of tissue to provide contrast in the images they produce. For example, while MRI uses differences in tissue magnetic properties, CT and film radiography produce images based on differences in the absorption of X-rays by different tissues. PET and SPECT rely on measuring the decay of radionuclides differentially absorbed by healthy and diseased tissue, whereas ultrasonography is based on detecting differences in the acoustic impedance (e.g., density or bulk modulus) between various tissues.

The properties of tissue involved in some typical radiographic imaging methods are shown in Fig. 2.1 and can be seen to vary by only about one order of magnitude, even between healthy and diseased tissues. This can limit the contrast and detectability of some tissues and structures. From the mechanical testing of ex vivo tissue samples, it has been shown that some tissue mechanical properties (e.g., the shear modulus) can vary over several orders of magnitude between different types of tissue and between normal and diseased tissues [9, 10]. Therefore, an imaging technique capable of measuring tissue mechanical properties could be quite sensitive to disease-related changes in these properties.

Elasticity Theory

Measuring and modeling the mechanical properties and behavior of materials is an important part of many fields of science. From improving the design of roads and buildings to creating artificial tissues and organs, knowledge of the mechanical properties of the individual components of a system and of the system as a whole are critical for the adequate performance of the final structure. Considerable research has been involved in the development of artificial tissues and organs, such as the heart, lung, liver, skin, and cartilage [11–14]. In some cases, the primary goal is to replicate the function of the original organ (e.g., the artificial heart). However, in other cases, reproducing the mechanical properties of the original tissue is

equally important because reproducing the mechanical response of the tissue under physiologic conditions will increase the chance that the patient will be able to return to normal activities with a normal range of motion and function. Therefore, understanding the mechanical properties of healthy and diseased tissue is important not only for diagnosing and characterizing a disease, but also for understanding and monitoring tissue function.

A number of mechanical tests exist for measuring the static and dynamic properties of materials (e.g., indentation, impact, creep, and torsion tests) [15–18]. These mechanical tests involve applying a known force (or stress) to the material and measuring the resulting displacement (or strain) of the material. For example, in an indentation test, a small probe is used to deform a small sample of a material. By measuring the amount of force that is being applied by the probe and the amount of deformation of the sample that results, material properties such as the Young's modulus, another indicator of material stiffness, can be determined. The response of a material during a particular test will depend on several mechanical properties, including anisotropic, nonlinear, thermal, geometric, composite, plastic, viscous, flow, and elastic effects. By carefully controlling the design of these experiments, and by making simplifying assumptions about the characteristics of the material and the applied stresses, the results of these measurements can be interpreted in meaningful ways (e.g., [17–31]).

A typical set of assumptions made when measuring the mechanical properties of a material is that of an infinite, homogeneous, linear, viscoelastic material [9, 32–34]. This set of assumptions significantly reduces the complexity of the mathematical relationship between the applied stresses and the resulting strains, and also reduces the number of unknown material properties that have to be determined to characterize the material. By assuming the material to be infinite, the impact of certain boundary conditions and boundary effects can be ignored. Assuming the material to be homogeneous (at least within a small region where data processing is performed) means only one set of material parameters needs to be considered and changes in the mechanical properties in space are negligible. Treating the material as linearly viscoelastic means that the strain of the material is linearly related to the applied stresses, though the response may change depending on the rate at which the stress is applied. Clearly, the validity of assumptions such as these must be reconsidered with every application because different materials and different experimental setups will have different characteristics.

Under the above assumptions, a fully anisotropic material may contain 21 independent quantities that would have to be known in order to fully characterize the material. The number of unknowns can be reduced by assuming that the material has certain symmetries. In a transversely isotropic material, the material is considered to have one preferential direction in which the response of the material is different from the response in the orthogonal directions. For example, in muscle, the response of muscle tissue along the direction of the muscle fibers to a particular stress will be different than the response of the tissue to a similar stress applied across the muscle fibers. Transversely isotropic materials can be described using as few as three parameters. Another common symmetry assumption is that the material under investigation is isotropic, and thus responds equally to stresses in any direction. An isotropic material only requires two quantities to describe its mechanical behavior, and several such quantities have been defined to aide in the description of the behavior of isotropic materials. These quantities include the Lamé parameters λ and μ (μ also being called the shear modulus), Poisson's ratio (ν), Young's modulus (E), the bulk modulus (K), and the P-wave modulus (M). Knowledge of any two of these quantities allows for the calculation of the others. For example, by knowing the shear modulus and Poisson's ratio, the others can be calculated as

$$\begin{aligned} E &= 2\mu(1+\nu), \quad \lambda = \frac{2\mu\nu}{1-2\nu}, \\ K &= \frac{2\mu(1+\nu)}{3(1-2\nu)}, \quad M = \frac{2\mu(1-\nu)}{1-2\nu}. \end{aligned} \tag{2.1}$$

To facilitate the analysis of the mechanical response of different types of materials under different loading conditions, the equations relating the stresses and strains can be expressed in different forms [9]. One such technique is to study the frequency-domain equations of motion for an infinite, isotropic, homogeneous, linear, viscoelastic material experiencing time-harmonic motion (such as a periodic deformation of tissue) [33]. These equations can be written as a set of complex-valued, coupled differential equations as

$$\begin{aligned} -\rho\omega^2 \boldsymbol{U}(\boldsymbol{r},f) &= (\lambda+\mu)\nabla\left(\nabla\cdot\boldsymbol{U}(\boldsymbol{r},f)\right) \\ &\quad +\mu\nabla^2\boldsymbol{U}(\boldsymbol{r},f) \\ &\text{or} \\ -\rho\omega^2 \boldsymbol{U}(\boldsymbol{r},f) &= (\lambda+2\mu)\nabla\left(\nabla\cdot\boldsymbol{U}(\boldsymbol{r},f)\right) \\ &\quad -\mu\nabla\times\left(\nabla\times\boldsymbol{U}(\boldsymbol{r},f)\right), \end{aligned} \tag{2.2}$$

where ρ is the density of the material, $\omega = 2\pi f$, f is the frequency of the harmonic motion, and $\boldsymbol{U}(\boldsymbol{r}, f)$ is the vector displacement of the material at the position $\boldsymbol{r}$. These equations can be used to show that, under the above assumptions, the response of the material is to propagate shear waves and longitudinal waves. Longitudinal waves have the property that the direction of the displacement of the material is in the same direction as the direction of wave propagation. Shear (or transverse) waves have the property that the displacement is perpendicular to the direction of wave propagation. The wave speed of the shear and longitudinal waves (c_S and c_L, respectively) can be written as

$$\begin{aligned} c_S &= \sqrt{\frac{2|\mu|^2}{\rho\left(\Re(\mu)+|\mu|\right)}} \xrightarrow{\Im(\mu)\to 0} \sqrt{\frac{\mu}{\rho}}, \\ c_L &= \sqrt{\frac{2|\lambda+2\mu|^2}{\rho\left(\Re(\lambda+2\mu)+|\lambda+2\mu|\right)}} \\ &\xrightarrow{\Im(\lambda+2\mu)\to 0} \sqrt{\frac{\lambda+2\mu}{\rho}}, \end{aligned} \tag{2.3}$$

where $|\mu|$, $R(\mu)$, and $I(\mu)$ indicate the magnitude, real part, and imaginary part of the complex-valued quantity μ, respectively.

It has been shown that the shear wave speed can vary significantly between different healthy and diseased tissues, from less than 1 m/s to over 100 m/s [10, 35, 36]. However, the longitudinal wave speed for most soft tissues is about 1,540 m/s and does not vary significantly between different types of tissue. Therefore, assessing the shear modulus and the shear wave speed has been the primary target for researchers trying to use the mechanical properties of tissue as indicators of disease.

Elasticity Imaging

Over the last 20 years, a number of imaging techniques have been developed to obtain information about the mechanical properties of tissue in vivo. Figure 2.2 provides a summary of the literature published on the topic of elasticity imaging over this time. This figure reflects the result of searching for "elastography" in the PubMed and Web of Knowledge databases for each publication year, ignoring false hits and conference abstracts, and differentiating the articles based on the primary imaging technique used or discussed. The imaging techniques, which will be discussed in more detail below, were crudely classified as [1] any ultrasound elasticity or strain imaging, [2] any phase-based MR elasticity or strain imaging, and [3] any other technique, including optical coherence tomography, X-ray, and MR tagging. While not an exhaustive or definitive search, the point of this figure is to indicate the rapid growth that the field of elasticity imaging has experienced, even in just the last 5 years in which the number of publications has doubled. This reflects the growing interest in the field and the rapid development of elasticity imaging techniques and applications.

Imaging the elastic properties of tissue involves several important steps. First, a static, transient, or harmonic force is applied to the tissue. Second, the resulting internal displacements of the tissue are measured. Third, the measured displacements are used to solve the equations of motion [e.g., Eq. (2.2)] that are assumed to model the behavior of the tissue to determine the mechanical properties of the tissue. Throughout the evolution of elasticity imaging, numerous approaches have been developed to

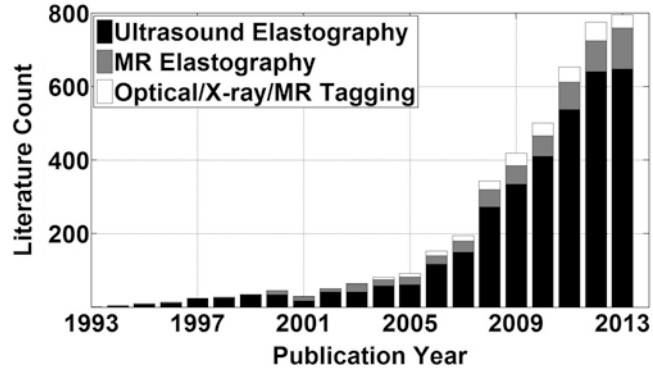

Fig. 2.2 A literature summary from searches in PubMed and Web of Knowledge using the search term "elastography." The results are roughly subdivided based on the primary imaging technique used or discussed

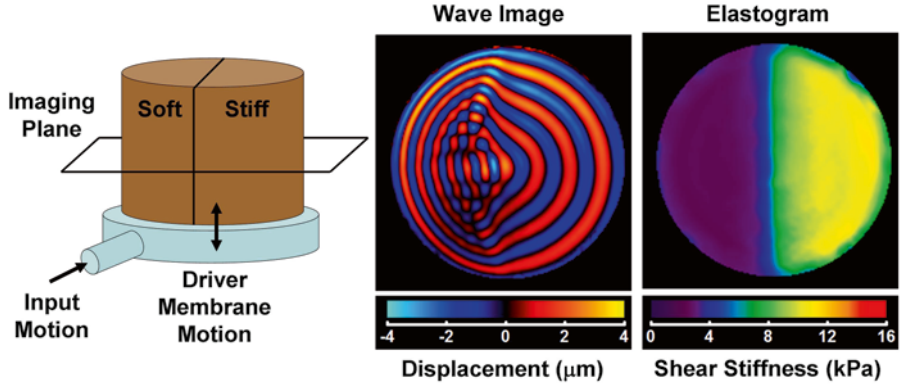

Fig. 2.3 Demonstration of elasticity imaging of a tissue-mimicking phantom. The cylindrical phantom consists of a soft half and a stiff half. The phantom is placed on top of a pneumatically powered drum that vibrates it vertically. Cross-sectional imaging is performed to measure the internal displacement field of the phantom, which provides pictures such as the one in the middle showing the through-plane component of the displacement field. The wave image shows shear waves propagating with a short wavelength through the soft material and a long wavelength in the stiff material. The wave images are used as the input into a wave equation modeling the wave propagation to solve for the stiffness of the phantom, as shown in the elastogram on the right

accomplish each of the above steps, each with its own benefits and limitations. Figure 2.3 shows a classic phantom experiment used to demonstrate these elasticity imaging principles.

The process of producing tissue motion can be performed using both extrinsic and intrinsic sources. Classic examples of extrinsic sources of motion include the use of piezoelectric elements, electromechanical actuators, and pneumatically powered drums and tubes that are placed in contact with the body [37, 38]. The vibrations produced by these external devices propagate into the body and throughout the tissue of interest. In contrast, changes in blood and CSF pressure, as well as the motion of the beating heart, can serve as sources of intrinsic motion and can produce motion directly within tissue [39–43]. Focused-ultrasound techniques, such as using amplitude modulation or interfering ultrasound beams, have also been employed as an external source of vibration that is capable of producing motion directly within tissue [44–50].

Tissue displacement can be measured in vivo using a number of techniques, including ultrasound, MRI, X-ray, and optical methods. A number of ultrasound-based methods for measuring

tissue motion have been used for elastographic imaging, including Doppler imaging and cross-correlation techniques [51–54]. These techniques have been used to image many different types of tissue, including muscle, skin, liver, breast, heart, prostate, and blood vessels. In Doppler-based ultrasound elasticity imaging, including "sono-elasticity," local tissue vibrations due to dynamic deformations cause Doppler shifts in the ultrasound signal which are used to measure tissue velocity changes over time [55–58]. The Doppler information can be used to obtain images showing wave propagation through tissue from which shear wavelengths and wave speeds can be obtained, which can be used to derive the elastic properties of the tissue [56, 59]. This record of tissue motion can also be used to calculate displacement and strain, as in the speckle-tracking techniques below, or it can be used with an appropriate equation of motion to directly solve for quantitative tissue mechanical properties. In speckle-tracking ultrasound elastography techniques, repeated ultrasound acquisitions are obtained while tissue is undergoing quasistatic or dynamic deformations [40, 60–63]. Cross-correlation analysis comparing successive images allows for estimates of the tissue displacement between the two acquisitions. The measured displacements can then be used to calculate strain maps (qualitative images of tissue elasticity) which are used to characterize the tissue [64–67] or to track wave propagation through the tissue for purposes of calculating the wave speed, which relates to tissue stiffness [62, 63]. The transient elastography method, also called Fibroscan, has become a very popular technique for quickly assessing hepatic fibrosis in vivo and noninvasively [62, 68]. Ultrasound elastography using ultrafast imaging techniques perform speckle-tracking to measure tissue displacement, but use customized hardware to acquire and reconstruct images at an effective frame rate of about 5,000 images per second [46, 63]. This method can image steady-state and transient wave propagation with high temporal and spatial resolutions and can be used to estimate tissue mechanical properties, including anisotropic and nonlinear properties [69, 70]. The primary limitations of these techniques are those produced by the ultrasound imaging itself in that an acoustic window is required to get the ultrasound signal into the tissue, the tissue displacement can typically only be measured in one direction (along the direction of the ultrasound beam), and the measurement depth is limited by the attenuation and scattering of the ultrasound beam.

Optical elastography methods have also been developed which are similar to speckle-tracking and Doppler ultrasound elastography, but use light instead of ultrasound to measure the tissue motion [71–76]. The higher resolution achievable with optical elastography makes it desirable for applications such as vascular imaging. However, like its ultrasound counterpart, this technique can only image tissue through an appropriate optical window, it can only measure displacements along the direction of the light beam, and it has significant depth limitations because of the high optical scattering and attenuation properties of tissue. Elastography techniques using X-rays have focused on acquiring static or quasistatic anatomical images and either using closed-form solutions to mechanical models of tissue deformation assuming certain geometries to determine mechanical properties, or using finite-element methods to iteratively adjust the assumed mechanical properties of a model until the model of the tissue behaves like the observed tissue deformation [77–80]. The X-ray and optical elastography techniques have not been as well developed as their ultrasound and MR counterparts.

Numerous MRI techniques have been developed over the years for measuring tissue motion and for determining the mechanical properties of tissue. Several methods have been developed which use the technique of spatial modulation of magnetization (SPAMM) to modulate the longitudinal magnetization of tissue to produce banding or grid patterns in the MR images that move with the deformation of the tissue [81–84]. From the MR images, the deformation of the grid pattern can be determined and used to estimate the strain distribution throughout the tissue. These techniques have been used for assessing cardiac and skeletal muscle function as well as for studying

intrinsic brain motion and models of traumatic brain injury [82, 85–90]. Like many of the speckle-tracking ultrasound and optical techniques, this technique only provides qualitative estimates of tissue mechanical properties unless additional assumptions are made about the tissue boundary conditions or the characteristics of the applied stresses. Another limitation of SPAMM techniques is that they typically require large-amplitude motion in order for the grid pattern to be tracked. While most SPAMM-based techniques produce in-plane grid patterns to measure tissue displacement, a similar approach using through-plane SPAMM tagging was developed in which the quasistatic compression of tissue can be used to produce strain-encoded images [91]. Because it does not actually track the motion of the SPAMM tags, this method is less computationally demanding than the conventional SPAMM technique, but it still only produces qualitative images of tissue mechanical properties.

In the SPAMM-based elastographic imaging techniques, tissue motion is calculated from a series of MR magnitude images. An alternative approach is to encode tissue motion into the phase of the MR signal. Normally, the magnetic field gradients used in MRI are used to determine the position of tissue that is assumed to be static. However, motion that occurs during these gradients will result in additional phase in the measured transverse magnetization according to

$$\varphi\left(\boldsymbol{r}_0,t\right)=\gamma\int_{t'=0}^{t'=t}\boldsymbol{G}\left(t'\right)\cdot\boldsymbol{u}\left(\boldsymbol{r}_0,t'\right)dt', \qquad (2.4)$$

where $\varphi(\boldsymbol{r}_0, t)$ is the motion-induced phase of tissue, originally at $\boldsymbol{r}_0$, at a time t after the creation of the transverse magnetization, γ is the proton gyromagnetic ratio, $\boldsymbol{G}(t)$ is the magnetic field gradient vector, and $\boldsymbol{u}(\boldsymbol{r}_0, t)$ models the motion of the tissue at $\boldsymbol{r}_0$ [92, 93]. This characteristic of the MR signal has been used for such applications as diffusion imaging, flow imaging, and compensating for flow artifacts [92–96].

Several MR elastography (MRE) techniques using phase-based motion encoding have been developed to measure the quasistatic and harmonic deformation of tissue. One of the MRE techniques developed involves the imaging of quasistatic tissue compression using a stimulated-echo MR acquisition [97–100]. Stimulated-echo MRE utilizes three RF pulses: the first RF pulse creates the transverse magnetization of the tissue while the tissue is in its initial state, the second RF pulse temporarily stores a portion of that signal as longitudinal magnetization while the tissue is deformed from its initial state (during the "mixing" time of the stimulated-echo sequence), and the third RF pulse returns the stored longitudinal magnetization to the transverse plane to be measured while the tissue is still in its deformed state. To determine the amount of motion that the tissue has experienced, motion-encoding gradient pulses are incorporated into the imaging sequence before and after the mixing time. For tissue that does not move during the mixing time, the effects of the motion-encoding gradients (MEG) cancel each other and no net phase shift is recorded. However, in regions where the tissue has moved, a phase shift will be recorded that is proportional to the amount of displacement that has occurred. Like the SPAMM technique, this record of the tissue displacement that is present in the MR images can be used to calculate the strain distribution within the tissue and to provide qualitative measures of tissue mechanical properties. To determine the tissue properties quantitatively, additional assumptions must be made about the boundary conditions and the stresses applied to the tissue.

An alternative form of MRE emerged from the desire to image the response of tissue to dynamic stresses [101, 102]. By using time-harmonic motion, equations of motion like Eq. (2.2) could be used to directly determine tissue mechanical properties, even without knowledge of the boundary conditions present during the acquisition. Early work showed that MR imaging sequences could be easily modified to be sensitive to periodic motion and that the properties of the acquisition could be tailored to enhance the sensitivity to motion at a particular frequency, or to yield broadband motion sensitivity, depending on the application [102–107]. Much like velocity encoding in MR vascular flow imaging, the motion sensitivity of MRE is accomplished by adding

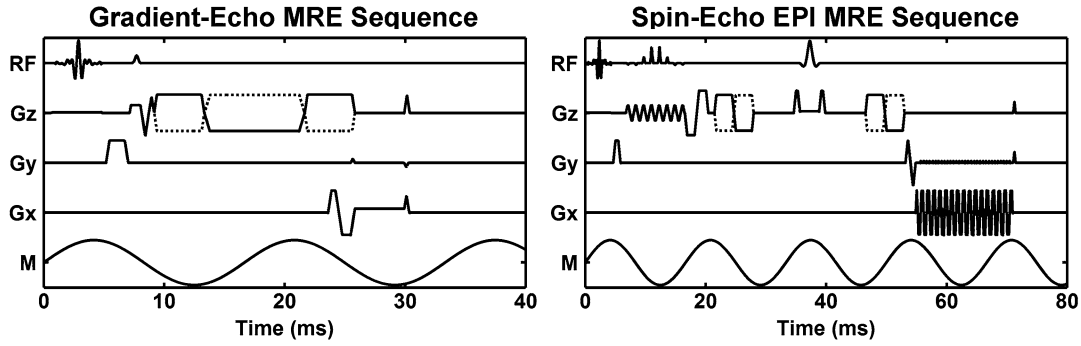

Fig. 2.4 Examples of gradient-echo MRE and spin-echo EPI MRE pulse sequences. The diagrams show the RF waveforms; the X, Y, and Z gradient waveforms, and the tissue motion ("M"). The MEG, indicated by the alternating polarity *solid* and *dashed curves* in each example, are shown applied in the Z direction to image just that component of the tissue motion. In general, the MEG can be applied along any combination of axes to record the component(s) of the motion needed for the analysis

additional MEG into standard MR imaging sequences which encode additional phase into the MR images in accordance with Eq. (2.4). Examples of MR imaging sequences which have been modified for MRE include gradient-recalled echo (GRE), spin echo (SE), echo planar imaging (EPI), balanced steady-state free precession (bSSFP), spiral, and stimulated-echo sequences [101–103, 106, 108–113]. Examples of GRE and SE-EPI MRE pulse sequences are shown in Fig. 2.4. Also like vascular flow imaging, MRE acquisitions are often repeated with two different amplitudes for the MEG (as indicated by the dashed MEG in Fig. 2.4). These two datasets are then combined to increase motion sensitivity while removing static phase errors from the images. In most applications, the MRE phase data are considered to be directly proportional to the tissue motion, thus the phase data can be substituted for displacement in equations of motion, such as Eq. (2.2), to determine the tissue mechanical properties.

Because the tissue motion in dynamic MRE is dynamic, the imaging sequence and the motion must be synchronized so that the timing, or phase relationship, between the motion and MEG remains constant during the acquisition. Each phase image produced in this fashion (also called a "wave image") is equivalent to imaging the dynamic displacement field at one instant in time. By changing the timing between the motion and MEG from one image acquisition to the next, multiple images ("phase offsets") can be obtained which show the propagation of the displacement field over time. The time-domain data can then either be processed directly, or analyzed in the Fourier domain to isolate the motion occurring at specific frequencies. Besides continuous periodic vibrations, the propagation of transient impulses through tissue can also be imaged. This technique has been pursued as an alternative means for measuring strain, stiffness, and other tissue properties, and has also been considered as a model for studying tissue response to traumatic injury [114–116].

Calculating Mechanical Properties

In order to determine the mechanical properties of tissue, the displacement data obtained from an elastographic imaging technique must be processed using algorithms based on appropriate equations of motion that characterize the tissue response to the applied stresses used during the acquisition. For MRE, numerous algorithms have been developed incorporating variational methods, finite-element models (FEM), level set techniques, and the direct solution of the differential equations of motion [117]. From one application

to another, different assumptions have to be made about the tissue, including assumptions about tissue anisotropy, compressibility, attenuation, dispersion, poroelasticity, and geometric effects (e.g., waveguide effects and wave scattering properties). The images that are obtained from these inversion algorithms, which indicate the distribution of tissue mechanical properties, are often referred to as elastograms. Using such algorithms, it is possible to estimate tissue properties such as the shear modulus, shear wave speed, and shear viscosity, as well as to produce images indicating tissue structural information such as anisotropy and the fluid–solid nature of the tissue.

For many elastography applications, tissue is assumed to be linearly elastic, homogeneous, and isotropic. These assumptions result in the approximation that the shear modulus μ of the tissue can be expressed as

$$\mu = \rho c_s^2 = \rho \left(\lambda f\right)^2, \tag{2.5}$$

where ρ is the density of the tissue, c_s is the shear wave speed in the tissue, λ is the shear wavelength, and f is the frequency of tissue vibration. If the tissue is dispersive, the shear modulus of the tissue changes with the frequency of vibration. Therefore, the shear modulus obtained using Eq. (2.5) for a particular frequency is only valid at that frequency, and this single-frequency estimate of the shear modulus is often called the shear stiffness. One way to determine the shear modulus from Eq. (2.5) is to estimate the shear wavelength from profiles extracted from the measured displacement data. Different techniques have been demonstrated for estimating the shear modulus in this fashion, including measuring the distance between peaks and troughs of the waves [118–120], fitting a sinusoid to the displacement data [48, 121], and fitting lines to the phase of complex-valued displacement data (the so-called "phase gradient" method) [122, 123]. While effective and straightforward to implement, these methods can be time consuming and error prone in the presence of interfering waves. A more sophisticated and robust method for measuring tissue stiffness was achieved with the implementation of the local frequency estimation (LFE) algorithm, which uses a series of image filters with different center frequencies and bandwidths to obtain automatic and isotropic estimates of stiffness [117, 124]. The multiscale nature of the LFE algorithm produces robust estimates of stiffness for heterogeneous media even in the presence of noise, making the technique appealing for a number of MRE applications, including kidney and prostate imaging [125–130]. However, the LFE technique can have lower spatial resolution than other techniques; often underestimates the stiffness of small, stiff structures; and lacks the ability to estimate the viscous properties of a material.

When the equations of motion governing tissue displacement are known, such as in Eq. (2.2), the tissue properties can sometimes be determined by directly substituting the measured displacements into the equations. This method is referred to as performing a direct inversion (DI) of the differential equations of motion [117, 131–135]. Because they are based directly on the equations of motion, DI algorithms can be designed that incorporate viscosity, anisotropy, and geometric effects [134, 136–139]. Also, since the analysis is typically performed on small, local regions of tissue, DI methods tend to have better spatial resolution than LFE methods. While DI methods are frequently applied to heterogeneous media, the inversions themselves typically assume that the mechanical properties of the medium are uniform within each processing window. This "local homogeneity" assumption is usually required for a practical solution of the equations of motion and is most valid when processing data within small regions away from boundaries and tissue interfaces. Since DI methods often require the calculation of high-order derivatives of noisy displacement data, when the data have low SNR, stiffness estimates provided by DI often have a larger variance than those produced by LFE. Careful consideration has to be made to the degree of data smoothing that is performed and the technique used to estimate the derivatives of the data to reduce the impact of noise on the final elastograms.

An alternative to directly inverting the differential equations of motion to obtain estimates of

material mechanical properties, which involves directly taking high-order derivatives of noisy data, are inversions which incorporate data models or smooth "test functions," so some of the derivatives are calculated on smooth analytic functions rather than noisy measured data. These techniques include classic variational methods as well as alternative formulations of the equations of motion that require fewer derivatives of the noisy data [135, 136, 140]. Variational methods, specifically, perform integration on the data while shifting the derivative calculations to well-behaved, smooth functions introduced partly to localize the inversion. While these methods would seem to be more robust to noise by design, in practice they are often implemented in a way that is equivalent to DI methods with some smoothing of the data, and thus they have only shown modest advantages over DI techniques. In contrast to techniques like DI and variational methods, which are often designed to ignore tissue geometry and heterogeneity, inversion algorithms based on the use of FEM have been designed which directly incorporate information about the tissue geometry and the full equations of motion [141–146]. In FEM inversions, a model is created using the imaged tissue geometry and motion, the equations of motion, an initial distribution of tissue mechanical properties, and an approximation for the boundary conditions. The FEM is then solved for the displacement field throughout the tissue. This displacement field is compared to the measured displacement field and the tissue mechanical properties in the model are then adjusted and the FEM is solved again. After a number of iterations, the distribution of tissue mechanical properties in the model converges to a final estimate of the tissue properties that produce a displacement field that is most similar to the measured displacements. This technique can be very robust to noise since it does not require the calculation of derivatives of noisy data, and it can more accurately model the wave propagation in tissue because it does not make the local homogeneity assumption required by other algorithms. However, it also requires an accurate model of the tissue motion, geometry, and boundary conditions for an accurate simulation, and this information can be difficult to obtain in practice. Also, because of the repeated evaluation of the FEM model, which may be very large for the general 3D case, these methods are often very time consuming.

The presence of interfering waves in the measured MRE displacement data can cause artifacts in some MRE inversion algorithms (e.g., the phase-gradient algorithm, DI methods, and LFE). This is because some algorithms implicitly or explicitly assume that the analysis is being performed on a single plane wave rather than a more complicated wave field with multiple interfering wave fronts, while the destructive interference that can arise from interfering waves causes numerical instabilities in other algorithms. A technique called directional filtering was developed to reduce these artifacts by using the temporal and spatial information in MRE data to separate waves propagating in different directions [147]. The extracted waves propagating in various directions each constitute a new displacement field on which the inversion algorithm can be applied to produce an estimate of tissue mechanical properties, and these multiple estimates of the mechanical properties can be averaged together to form the final elastogram. Additional low-pass and high-pass filtering properties can be incorporated into the directional filters to reduce image noise and the effects of longitudinal wave propagation and tissue bulk motion, both of which tend to introduce long wavelength information into the measured displacement data. Longitudinal wave motion can be better removed from the data by calculating the vector curl of the measured wave field, though this is not always possible as it requires the measurement of the full 3D vector wave field, which may be too time consuming in some applications [109, 148, 149]. An alternative approach to the directional filter for reducing the effects of interfering waves is to design a model of the wave propagation that incorporates waves propagating in many different directions and solves for them simultaneously [136]. Additional improvements in the visualization of tissue mechanical properties can be obtained by incorporating data measured using different mechanical vibration frequencies. The wave fields produced by different vibration frequencies

have different regions of wave interference. Merging the different wave fields in one inversion compensates for this wave interference and improves the overall depiction of the tissue properties [107, 136]. One limitation of this method, however, is that it assumes that the tissue mechanical properties are the same at these different vibration frequencies. Due to dispersive effects in the tissue, this is not true. However, the difference in properties may be small enough over a small enough bandwidth of frequencies that the error in this type of tissue model is insignificant to the overall improvement in the way the tissue properties are depicted.

Summary

The field of elasticity imaging has evolved tremendously over the last 30 years and has included significant developments at every level, from improvements in how motion is created in vivo and what types of motion can be imaged, to how the imaging of tissue motion is performed, to how the images of tissue motion are processed to reveal tissue mechanical properties. In MRE, these developments have allowed for the in vivo evaluation of the liver, spleen, kidneys, brain, breast, skeletal muscle, and heart, among other applications, to assess their normal properties and how these mechanical properties change with the progression of various diseases. The rest of this book will discuss the current state of the art in MRE applications for imaging these various organs.

References

1. Field D. Anatomy: palpation and surface markings. 3rd ed. Oxford: Butterworth Heinemann; 2001.
2. Bickley LS, Szilagyi PG. Bates' guide to physical examination and history taking. 8th ed. Philadelphia: Lippincott Williams & Wilkins; 2003.
3. Mangione S. Physical diagnosis secrets. 2nd ed. Philadelphia: Mosby/Elsevier; 2008.
4. Bacon BR, O'Grady JG, Di Bisceglie AM, Lake JR. Comprehensive clinical hepatology. 2nd ed. Philadelphia: Elsevier Limited; 2006.
5. Barton MB, Harris R, Fletcher SW. Does this patient have breast cancer? The screening clinical breast examination: should it be done? How? JAMA. 1999;282(13):1270–80.
6. Roubidoux MA, Bailey JE, Wray LA, Helvie MA. Invasive cancers detected after breast cancer screening yielded a negative result: relationship of mammographic density to tumor prognostic factors. Radiology. 2004;230(1):42–8.
7. Roubidoux MA, Wilson TE, Orange RJ, Fitzgerald JT, Helvie MA, Packer SA. Breast cancer in women who undergo screening mammography: relationship of hormone replacement therapy to stage and detection method. Radiology. 1998;208(3):725–8.
8. Guimaraes CM, Correia MM, Baldisserotto M, Aires EPD, Coelho JF. Intraoperative ultrasonography of the liver in patients with abdominal tumors - a new approach. J Ultrasound Med. 2004;23(12):1549–55.
9. Fung YC. Biomechanics: mechanical properties of living tissues. 2nd ed. New York: Springer; 1993.
10. Duck FA. Physical properties of tissue: a comprehensive reference book. London: Academic; 1990.
11. Holzapfel BM, Reichert JC, Schantz JT, Gbureck U, Rackwitz L, Noth U, etal. How smart do biomaterials need to be? A translational science and clinical point of view. Adv Drug Deliv Rev. 2013;65(4):581–603.
12. Tritto G, Davies NA, Jalan R. Liver replacement therapy. Semin Respir Crit Care Med. 2012;33(1):70–9.
13. Malchesky PS. Artificial organs 2011: a year in review. Artif Organs. 2012;36(3):291–323.
14. Atala A. Engineering organs. Curr Opin Biotechnol. 2009;20(5):575–92.
15. Yang F, Li JCM. Impression test – a review. Mater Sci Eng R. 2013;74(8):233–53.
16. Walley SM. Historical origins of indentation hardness testing. Mater Sci Technol. 2012;28(9–10):1028–44.
17. Lakes RS. Viscoelastic materials. Cambridge: Cambridge University Press; 2009.
18. Nerurkar NL, Elliott DM, Mauck RL. Mechanical design criteria for intervertebral disc tissue engineering. J Biomech. 2010;43(6):1017–30.
19. Laksari K, Shafieian M, Darvish K. Constitutive model for brain tissue under finite compression. J Biomech. 2012;45(4):642–6.
20. Sparrey CJ, Keaveny TM. Compression behavior of porcine spinal cord white matter. J Biomech. 2011; 44(6):1078–82.
21. Stokes IA, Laible JP, Gardner-Morse MG, Costi JJ, Iatridis JC. Refinement of elastic, poroelastic, and osmotic tissue properties of intervertebral disks to analyze behavior in compression. Ann Biomed Eng. 2011;39(1):122–31.
22. Hatami-Marbini H, Etebu E. An experimental and theoretical analysis of unconfined compression of corneal stroma. J Biomech. 2013;46(10):1752–8.
23. Mansour JM, Welter JF. Multimodal evaluation of tissue-engineered cartilage. J Med Biol Eng. 2013; 33(1):1–16.
24. Van Loocke M, Lyons CG, Simms CK. Viscoelastic properties of passive skeletal muscle in compression: stress-relaxation behaviour and constitutive modelling. J Biomech. 2008;41(7):1555–66.

25. Chen DL, Yang PF, Lai YS. A review of three-dimensional viscoelastic models with an application to viscoelasticity characterization using nanoindentation. Microelectron Reliab. 2012;52(3):541–58.
26. O'Connor WT, Smyth A, Gilchrist MD. Animal models of traumatic brain injury: a critical evaluation. Pharmacol Ther. 2011;130(2):106–13.
27. Lin YC, Chen XM.A critical review of experimental results and constitutive descriptions for metals and alloys in hot working. Mater Des. 2011;32(4): 1733–59.
28. Murphy JG. Transversely isotropic biological, soft tissue must be modelled using both anisotropic invariants. Eur J Mech-A/Solids. 2013;42:90–6.
29. Cowin SC. Bone poroelasticity. J Biomech. 1999; 32(3):217–38.
30. Darvish KK, Crandall JR. Nonlinear viscoelastic effects in oscillatory shear deformation of brain tissue. Med Eng Phys. 2001;23(9):633–45.
31. Hasan A, Ragaert K, Swieszkowski W, Selimovic S, Paul A, Camci-Unal G, et al. Biomechanical properties of native and tissue engineered heart valve constructs. J Biomech. 2013;47(9):1949–63. doi:10.1016/j.jbiomech.2013.09.023 Oct 21.
32. Aki K, Richards PG. Quantitative seismology. 2nd ed. Sausalito: University Science; 2002.
33. Oestreicher HL. Field and impedance of an oscillating sphere in a viscoelastic medium with application to biophysics. J Acoust Soc Am. 1951;23(6):707–14.
34. Auld BA. Acoustic fields and waves in solids. 2nd ed. Malabar: Krieger; 1990.
35. Sarvazyan AP, Skovoroda AR, Emelianov SY, Fowlkes JB, Pipe JG, Adler RS, et al. Biophysical bases of elasticity imaging. In: Jones JP, editor. Acoustical imaging. New York: Plenum; 1995. p. 223–40.
36. Krouskop TA, Wheeler TM, Kallel F, Garra BS, Hall T. Elastic moduli of breast and prostate tissues under compression. Ultrason Imaging. 1998;20(4):260–74.
37. Uffmann K, Ladd ME. Actuation systems for MR elastography: design and applications. IEEE Eng Med Biol Mag. 2008;27(3):28–34.
38. Tse ZT, Janssen H, Hamed A, Ristic M, Young I, Lamperth M. Magnetic resonance elastography hardware design: a survey. Proc Inst Mech Eng H. 2009;223(4):497–514.
39. Dighe M, Bae U, Richardson ML, Dubinsky TJ, Minoshima S, Kim Y. Differential diagnosis of thyroid nodules with US elastography using carotid artery pulsation. Radiology. 2008;248(2):662–9.
40. Konofagou EE, D'Hooge J, Ophir J. Myocardial elastography – a feasibility study in vivo. Ultrasound Med Biol. 2002;28(4):475–82.
41. Hirsch S, Klatt D, Freimann F, Scheel M, Braun J, Sack I. In vivo measurement of volumetric strain in the human brain induced by arterial pulsation and harmonic waves. Magn Reson Med. 2013;70(3):671–83.
42. Kolen AF, Miller NR, Ahmed EE, Bamber JC. Characterization of cardiovascular liver motion for the eventual application of elasticity imaging to the liver in vivo. Phys Med Biol. 2004;49(18): 4187–206.
43. Chung S, Breton E, Mannelli L, Axel L. Liver stiffness assessment by tagged MRI of cardiac-induced liver motion. Magn Reson Med. 2011;65(4):949–55.
44. Nightingale K, Soo MS, Nightingale R, Trahey G. Acoustic radiation force impulse imaging: in vivo demonstration of clinical feasibility. Ultrasound Med Biol. 2002;28(2):227–35.
45. Sarvazyan AP, Rudenko OV, Swanson SD, Fowlkes JB, Emelianov SY. Shear wave elasticity imaging: a new ultrasonic technology of medical diagnostics. Ultrasound Med Biol. 1998;24(9):1419–35.
46. Sinkus R, Tanter M, Bercoff J, Siegmann K, Pernot M, Athanasiou A, et al. Potential of MRI and ultrasound radiation force in elastography: applications to diagnosis and therapy. Proc IEEE. 2008;96(3):490–9.
47. McDannold N, Maier SE. Magnetic resonance acoustic radiation force imaging. Med Phys. 2008; 35(8):3748–58.
48. Wu T, Felmlee JP, Greenleaf JF, Riederer SJ, Ehman RL. MR imaging of shear waves generated by focused ultrasound. Magn Reson Med. 2000;43(1):111–5.
49. Greenleaf JF, Fatemi M, Insana M. Selected methods for imaging elastic properties of biological tissues. Annu Rev Biomed Eng. 2003;5:57–78.
50. Chen S, Urban MW, Pislaru C, Kinnick R, Zheng Y, Yao A, et al. Shearwave dispersion ultrasound vibrometry (SDUV) for measuring tissue elasticity and viscosity. IEEE Trans Ultrason Ferroelectr Freq Control. 2009;56(1):55–62.
51. Parker KJ, Doyley MM, Rubens DJ. Imaging the elastic properties of tissue: the 20 year perspective. Phys Med Biol. 2011;56:R1–29.
52. Wells PN, Liang HD. Medical ultrasound: imaging of soft tissue strain and elasticity. J R Soc Interface. 2011;8(64):1521–49.
53. Sporea I, Gilja OH, Bota S, Sirli R, Popescu ALiver elastography – an update. Med Ultrason. 2013; 15(4):304–14.
54. Castaneda B, Ormachea J, Rodriguez P, Parker KJ. Application of numerical methods to elasticity imaging. Mol Cell Biomech: MCB. 2013;10(1): 43–65.
55. Krouskop TA, Dougherty DR, Vinson FS. A pulsed Doppler ultrasonic system for making noninvasive measurements of the mechanical properties of soft tissue. J Rehabil Res Dev. 1987;24(2):1–8.
56. Yamakoshi Y, Sato J, Sato T. Ultrasonic imaging of internal vibration of soft tissue under forced vibration. IEEE Trans Ultrason Ferroelectr Freq Control. 1990;37(2):45–53.
57. Lerner RM, Huang SR, Parker KJ. "Sonoelasticity" images derived from ultrasound signals in mechanically vibrated tissues. Ultrasound Med Biol. 1990; 16(3):231–9.
58. Parker KJ, Huang SR, Musulin RA, Lerner RM. Tissue response to mechanical vibrations for "sonoelasticity imaging". Ultrasound Med Biol. 1990;16(3):241–6.
59. Sanada M, Ebara M, Fukuda H, Yoshikawa M, Sugiura N, Saisho H, et al. Clinical evaluation of sonoelasticity measurement in liver using ultrasonic

imaging of internal forced low-frequency vibration. Ultrasound Med Biol. 2000;26(9):1455–60.
60. Ophir J, Cespedes I, Ponnekanti H, Yazdi Y, Li X. Elastography: a quantitative method for imaging the elasticity of biological tissues. Ultrason Imaging. 1991;13(2):111–34.
61. Ophir J, Kallel F, Varghese T, Konofagou E, Alam SK, Krouskop T, et al. Elastography. C R Acad Sci Ser IV-Phys Astr. 2001;2(8):1193–212.
62. Sandrin L, Fourquet B, Hasquenoph JM, Yon S, Fournier C, Mal F, et al. Transient elastography: a new noninvasive method for assessment of hepatic fibrosis. Ultrasound Med Biol. 2003;29(12):1705–13.
63. Sandrin L, Tanter M, Catheline S, Fink M. Shear modulus imaging with 2-D transient elastography. IEEE Trans Ultrason Ferroelectr Freq Control. 2002;49(4):426–35.
64. Righetti R, Righetti M, Ophir J, Krouskop TA. The feasibility of estimating and imaging the mechanical behavior of poroelastic materials using axial strain elastography. Phys Med Biol. 2007;52(11):3241–59.
65. Ophir J, Srinivasan S, Righetti R, Thittai A. Elastography: a decade of progress (2000–2010). Curr Med Imaging Rev. 2011;7(4):292–312.
66. Cespedes I, Ophir J, Ponnekanti H, Maklad N. Elastography: elasticity imaging using ultrasound with application to muscle and breast in vivo. Ultrason Imaging. 1993;15(2):73–88.
67. Ophir J, Alam SK, Garra BS, Kallel F, Konofagou EE, Krouskop T, et al. Elastography: imaging the elastic properties of soft tissues with ultrasound. J Med Ultrason. 2002;29:155–71.
68. Jung KS, Kim SU. Clinical applications of transient elastography. Clin Mol Hepatol. 2012;18(2):163–73.
69. Gennisson JL, Grenier N, Combe C, Tanter M. Supersonic shear wave elastography of in vivo pig kidney: influence of blood pressure, urinary pressure and tissue anisotropy. Ultrasound Med Biol. 2012;38(9):1559–67.
70. Sinkus R, Bercoff J, Tanter M, Gennisson JL, El Khoury C, Servois V, et al. Nonlinear viscoelastic properties of tissue assessed by ultrasound. IEEE Trans Ultrason Ferroelectr Freq Control. 2006; 53(11):2009–18.
71. Kirkpatrick SJ, Wang RK, Duncan DD, Kulesz-Martin M, Lee K. Imaging the mechanical stiffness of skin lesions by in vivo acousto-optical elastography. Opt Express. 2006;14(21):9770–9.
72. Wang RKK, Ma ZH, Kirkpatrick SJ. Tissue Doppler optical coherence elastography for real time strain rate and strain mapping of soft tissue. Appl Phys Lett. 2006;89(14):144103.
73. Rogowska J, Patel N, Plummer S, Brezinski ME. Quantitative optical coherence tomographic elastography: method for assessing arterial mechanical properties. Br J Radiol. 2006;79(945):707–11.
74. Kennedy KM, McLaughlin RA, Kennedy BF, Tien A, Latham B, Saunders CM, et al. Needle optical coherence elastography for the measurement of microscale mechanical contrast deep within human breast tissues. J Biomed Opt. 2013;18(12):121510.
75. Wang S, Larin KV. Shear wave imaging optical coherence tomography (SWI-OCT) for ocular tissue biomechanics. Opt Lett. 2014;39(1):41–4.
76. Nahas A, Tanter M, Nguyen TM, Chassot JM, Fink M, Claude BA. From supersonic shear wave imaging to full-field optical coherence shear wave elastography. J Biomed Opt. 2013;18(12):121514.
77. Lee MK, Drangova M, Holdsworth DW, Fenster A. Application of dynamic computed tomography for measurements of local aortic elastic modulus. Med Biol Eng Comput. 1999;37(1):13–24.
78. Wang ZG, Liu Y, Wang G, Sun LZ. Nonlinear elastomammography for characterization of breast tissue properties. Int J Biomed Imaging. 2011;2011:10. 540820.
79. Wang ZG, Liu Y, Sun LZ, Wang G, Fajardo LLElastomammography: theory, algorithm, and phantom study. Int J Biomed Imaging. 2006;2006:53050.
80. Drangova M, Holdsworth DW, Boyd CJ, Dunmore PJ, Roach MR, Fenster A. Elasticity and geometry measurements of vascular specimens using a high-resolution laboratory CT scanner. Physiol Meas. 1993;14(3):277–90.
81. Axel L, Dougherty L. Heart wall motion: improved method of spatial modulation of magnetization for MR imaging. Radiology. 1989;172(2):349–50.
82. Osman NF, Kerwin WS, McVeigh ER, Prince JL. Cardiac motion tracking using CINE harmonic phase (HARP) magnetic resonance imaging. Magn Reson Med. 1999;42(6):1048–60.
83. Wang H, Amini AA. Cardiac motion and deformation recovery from MRI: a review. IEEE Trans Med Imaging. 2012;31(2):487–503.
84. Creswell LL, Moulton MJ, Wyers SG, Pirolo JS, Fishman DS, Perman WH, et al. An experimental method for evaluating constitutive models of myocardium in in vivo hearts. Am J Physiol. 1994;267 (2 Pt 2):H853–63.
85. Yeon SB, Reichek N, Tallant BA, Lima JA, Calhoun LP, Clark NR, et al. Validation of invivo myocardial strain measurement by magnetic resonance tagging with sonomicrometry. J Am Coll Cardiol. 2001; 38(2):555–61.
86. Gotte MJ, Germans T, Russel IK, Zwanenburg JJ, Marcus JT, van Rossum AC, et al. Myocardial strain and torsion quantified by cardiovascular magnetic resonance tissue tagging: studies in normal and impaired left ventricular function. J Am Coll Cardiol. 2006;48(10):2002–11.
87. Sabet AA, Christoforou E, Zatlin B, Genin GM, Bayly PV. Deformation of the human brain induced by mild angular head acceleration. J Biomech. 2008;41(2):307–15.
88. Soellinger M, Ryf S, Boesiger P, Kozerke S. Assessment of human brain motion using CSPAMM. J Magn Reson Imaging. 2007;25(4):709–14.
89. Fu YB, Chui CK, Teo CL, Kobayashi E. Motion tracking and strain map computation for quasi-static magnetic resonance elastography. Med Image Comput Comput Assist Interv. 2011;14(Pt 1): 428–35.

90. Ceelen KK, Stekelenburg A, Mulders JL, Strijkers GJ, Baaijens FP, Nicolay K, et al. Validation of a numerical model of skeletal muscle compression with MR tagging: a contribution to pressure ulcer research. J Biomech Eng. 2008;130(6):061015.
91. Osman NF. Detecting stiff masses using strain-encoded (SENC) imaging. Magn Reson Med. 2003;49(3):605–8.
92. Bernstein MA, King KF, Zhou ZJ. Handbook of MRI pulse sequences. Burlington: Elsevier Academic; 2004.
93. Haacke EM. Magnetic resonance imaging: physical principles and sequence design. New York: Wiley; 1999.
94. Singer JR. NMR diffusion and flow measurements and an introduction to spin phase graphing. J Phys E. 1978;11:281–91.
95. Dumoulin CL, Hart Jr HR. Magnetic resonance angiography. Radiology. 1986;161(3):717–20.
96. Nayler GL, Firmin DN, Longmore DB. Blood flow imaging by cine magnetic resonance. J Comput Assist Tomogr. 1986;10(5):715–22.
97. Chenevert TL, Skovoroda AR, O'Donnell M, Emelianov SY. Elasticity reconstructive imaging by means of stimulated echo MRI. Magn Reson Med. 1998;39(3):482–90.
98. Plewes DB, Bishop J, Samani A, Sciarretta J. Visualization and quantification of breast cancer biomechanical properties with magnetic resonance elastography. Phys Med Biol. 2000;45(6):1591–610.
99. Hardy PA, Ridler AC, Chiarot CB, Plewes DB, Henkelman RM. Imaging articular cartilage under compression-cartilage elastography. Magn Reson Med. 2005;53(5):1065–73.
100. Siegler P, Jenne JW, Boese JM, Huber PE, Schad LR. STEAM-sequence with multi-echo-readout for static magnetic resonance elastography. Z Med Phys. 2007;17(2):118–26.
101. Muthupillai R, Lomas DJ, Rossman PJ, Greenleaf JF, Manduca A, Ehman RL. Magnetic resonance elastography by direct visualization of propagating acoustic strain waves. Science. 1995;269(5232):1854–7.
102. Muthupillai R, Rossman PJ, Lomas DJ, Greenleaf JF, Riederer SJ, Ehman RL. Magnetic resonance imaging of transverse acoustic strain waves. Magn Reson Med. 1996;36(2):266–74.
103. Rump J, Klatt D, Braun J, Warmuth C, Sack I. Fractional encoding of harmonic motions in MR elastography. Magn Reson Med. 2007;57(2):388–95.
104. Lewa CJ. Magnetic resonance imaging in the presence of mechanical waves: NMR frequency modulation, mechanical waves as NMR factor, local temperature variations. Spectrosc Lett. 1991;24(1):55–67.
105. Lewa CJ, de Certaines JD. MR imaging of viscoelastic properties. J Magn Reson Imaging. 1995;5(2):242–4.
106. Garteiser P, Sahebjavaher RS, Ter Beek LC, Salcudean S, Vilgrain V, Van Beers BE, et al. Rapid acquisition of multifrequency, multislice and multidirectional MR elastography data with a fractionally encoded gradient echo sequence. NMR Biomed. 2013;26(10):1326–35.
107. Hirsch S, Guo J, Reiter R, Papazoglou S, Kroencke T, Braun J, et al. MR elastography of the liver and the spleen using a piezoelectric driver, single-shot wave-field acquisition, and multifrequency dual parameter reconstruction. Magn Reson Med. 2014;71(1):267–77.
108. Glaser KJ, Felmlee JP, Ehman RL. Rapid MR elastography using selective excitations. Magn Reson Med. 2006;55(6):1381–9.
109. Sinkus R, Tanter M, Catheline S, Lorenzen J, Kuhl C, Sondermann E, et al. Imaging anisotropic and viscous properties of breast tissue by magnetic resonance-elastography. Magn Reson Med. 2005;53(2):372–87.
110. Maderwald S, Uffmann K, Galban CJ, de Greiff A, Ladd ME. Accelerating MR elastography: a multi-echo phase-contrast gradient-echo sequence. J Magn Reson Imaging. 2006;23(5):774–80.
111. Bieri O, Maderwald S, Ladd ME, Scheffler K. Balanced alternating steady-state elastography. Magn Reson Med. 2006;55(2):233–41.
112. Huwart L, Salameh N, Ter Beek L, Vicaut E, Peeters F, Sinkus R, et al. MR elastography of liver fibrosis: preliminary results comparing spin-echo and echo-planar imaging. Eur Radiol. 2008;18(11):2535–41.
113. Johnson CL, McGarry MD, Van Houten EE, Weaver JB, Paulsen KD, Sutton BP, et al. Magnetic resonance elastography of the brain using multishot spiral readouts with self-navigated motion correction. Magn Reson Med. 2013;70(2):404–12.
114. McCracken PJ, Manduca A, Felmlee J, Ehman RL. Mechanical transient-based magnetic resonance elastography. Magn Reson Med. 2005;53(3):628–39.
115. Gallichan D, Robson MD, Bartsch A, Miller KL. TREMR: table-resonance elastography with MR. Magn Reson Med. 2009;62(3):815–21.
116. Souchon R, Salomir R, Beuf O, Milot L, Grenier D, Lyonnet D, et al. Transient MR elastography (t-MRE) using ultrasound radiation force: theory, safety, and initial experiments in vitro. Magn Reson Med. 2008;60(4):871–81.
117. Manduca A, Oliphant TE, Dresner MA, Mahowald JL, Kruse SA, Amromin E, et al. Magnetic resonance elastography: non-invasive mapping of tissue elasticity. Med Image Anal. 2001;5(4):237–54.
118. Leclerc GE, Charleux F, Robert L, Ho Ba Tho MC, Rhein C, Latrive JP, et al. Analysis of liver viscosity behavior as a function of multifrequency magnetic resonance elastography (MMRE) postprocessing. J Magn Reson Imaging. 2013;38(2):422–8.
119. McCullough MB, Domire ZJ, Reed AM, Amin S, Ytterberg SR, Chen Q, et al. Evaluation of muscles affected by myositis using magnetic resonance elastography. Muscle Nerve. 2011;43(4):585–90.
120. Xu L, Chen J, Yin M, Glaser KJ, Chen Q, Woodrum DA, et al. Assessment of stiffness changes in the

ex vivo porcine aortic wall using magnetic resonance elastography. Magn Reson Imaging. 2012;30(1): 122–7.
121. Dresner MA, Rose GH, Rossman PJ, Muthupillai R, Manduca A, Ehman RL. Magnetic resonance elas - tography of skeletal muscle. J Magn Reson Imaging. 2001;13(2):269–76.
122. Yin M, Woollard J, Wang XF, Torres VE, Harris PC, Ward CJ, et al. Quantitative assessment of hepatic fibrosis in an animal model with magnetic resonance elastography. Magn Reson Med. 2007;58(2): 346–53.
123. Kolipaka A, Aggarwal SR, McGee KP, Anavekar N, Manduca A, Ehman RL, et al. Magnetic resonance elastography as a method to estimate myocardial contractility. J Magn Reson Imaging. 2012; 36(1):120–7.
124. Knutsson H, Westin CF, Granlund G. Local multi - scale frequency and bandwidth estimation. Proc IEEE Int Conf Image Process. 1994;1:36–40.
125. Bensamoun SF, Robert L, Leclerc GE, Debernard L, Charleux F. Stiffness imaging of the kidney and adjacent abdominal tissues measured simultaneously using magnetic resonance elastography. Clin Imaging. 2011;35(4):284–7.
126. Rouviere O, Souchon R, Pagnoux G, Menager JM, Chapelon JY. Magnetic resonance elastography of the kidneys: feasibility and reproducibility in young healthy adults. J Magn Reson Imaging. 2011; 34(4):880–6.
127. Braun J, Buntkowsky G, Bernarding J, Tolxdorff T, Sack I. Simulation and analysis of magnetic resonance elastography wave images using coupled harmonic oscillators and Gaussian local frequency estimation. Magn Reson Imaging. 2001;19(5): 703–13.
128. Clayton EH, Okamoto RJ, Bayly PV. Mechanical properties of viscoelastic media by local frequency estimation of divergence-free wave fields. J Biomech Eng. 2013;135(2):021025.
129. Sahebjavaher RS, Baghani A, Honarvar M, Sinkus R, Salcudean SE. Transperineal prostate MR elastography: initial in vivo results. Magn Reson Med. 2013; 69(2):411–20.
130. Li BN, Chui CK, Ong SH, Numano T, Washio T, Homma K, et al. Modeling shear modulus distribution in magnetic resonance elastography with piecewise constant level sets. Magn Reson Imaging. 2012;30(3):390–401.
131. Oliphant TE, Manduca A, Ehman RL, Greenleaf JF. Complex-valued stiffness reconstruction for magnetic resonance elastography by algebraic inversion of the differential equation. Magn Reson Med. 2001;45(2):299–310.
132. Papazoglou S, Hirsch S, Braun J, Sack I. Multifrequency inversion in magnetic resonance elastography. Phys Med Biol. 2012;57(8):2329–46.
133. Boulet T, Kelso ML, Othman SF. Microscopic magnetic resonance elastography of traumatic brain injury model. J Neurosci Methods. 2011;201(2): 296–306.
134. Doyley MM. Model-based elastography: a survey of approaches to the inverse elasticity problem. Phys Med Biol. 2012;57(3):R35–73.
135. Romano AJ, Bucaro JA, Ehman RL, Shirron JJ. Evaluation of a material parameter extraction algorithm using MRI-based displacement measurement. IEEE Trans Ultrason Ferroelectr Freq Control. 2000;47(6):1575–81.
136. Baghani A, Salcudean S, Honarvar M, Sahebjavaher RS, Rohling R, Sinkus R. Travelling wave expansion: a model fitting approach to the inverse problem of elasticity reconstruction. IEEE Trans Med Imaging. 2011;30(8):1555–65.
137. Romano A, Scheel M, Hirsch S, Braun J, Sack I. In vivo waveguide elastography of white matter tracts in the human brain. Magn Reson Med. 2012; 68(5):1410–22.
138. Kolipaka A, McGee KP, Araoz PA, Glaser KJ, Manduca A, Romano AJ, et al. MR elastography as a method for the assessment of myocardial stiffness: comparison with an established pressure–volume model in a left ventricular model of the heart. Magn Reson Med. 2009;62(1):135–40.
139. McLaughlin JR, Zhang N, Manduca A. Calculating tissue shear modulus and pressure by 2D log-elastographic methods. Inverse Prob. 2010;26(8): 085007.
140. Kwon OI, Park C, Nam HS, Woo EJ, Seo JK, Glaser KJ, et al. Shear modulus decomposition algorithm in magnetic resonance elastography. IEEE Trans Med Imaging. 2009;28(10):1526–33.
141. Perreard IM, Pattison AJ, Doyley M, McGarry MD, Barani Z, Van Houten EE, et al. Effects of frequency- and direction-dependent elastic materials on linearly elastic MRE image reconstructions. Phys Med Biol. 2010;55(22):6801–15.
142. Litwiller DV, Lee SJ, Kolipaka A, Mariappan YK, Glaser KJ, Pulido JS, et al. MR elastography of the ex vivo bovine globe. J Magn Reson Imaging. 2010;32(1):44–51.
143. Van Houten EEW, Miga MI, Weaver JB, Kennedy FE, Paulsen KD. Three-dimensional subzone-based reconstruction algorithm for MR elastography. Magn Reson Med. 2001;45(5):827–37.
144. McGarry MD, Van Houten EE, Johnson CL, Georgiadis JG, Sutton BP, Weaver JB, et al. Multiresolution MR elastography using nonlinear inversion. Med Phys. 2012;39(10):6388–96.
145. Perrinez PR, Kennedy FE, Van Houten EE, Weaver JB, Paulsen KD. Modeling of soft poroelastic tissue in time-harmonic MR elastography. IEEE Trans Biomed Eng. 2009;56(3):598–608.
146. Perrinez PR, Kennedy FE, Van Houten EE, Weaver JB, Paulsen KD. Magnetic resonance poroelastography: an algorithm for estimating the mechanical properties of fluid-saturated soft tissues. IEEE Trans Med Imaging. 2010;29(3):746–55.

147. Manduca A, Lake DS, Kruse SA, Ehman RL. Spatio-temporal directional filtering for improved inversion of MR elastography images. Med Image Anal. 2003;7(4):465–73.
148. Honarvar M, Sahebjavaher R, Sinkus R, Rohling R, Salcudean S. Curl-based finite element reconstruction of the shear modulus without assuming local homogeneity: time harmonic case. IEEE Trans Med Imaging. 2013;32(12):2189–99.
149. Baghani A, Salcudean S, Rohling R. Theoretical limitations of the elastic wave equation inversion for tissue elastography. J Acoust Soc Am. 2009;126(3):1541.